Lithium ionic conduction in composites of $Li(BH_4)_{0.75}I_{0.25}$ and amorphous $0.75Li_2S{\cdot}0.25P_2S_5$ for battery applications

Abdel El kharbachi[a], Yang Hu[b], Koji Yoshida[c], Ponniah Vajeeston[b], Sangryun Kim[c], Magnus H. Sørby[a], Shin-ichi Orimo[c,d], Helmer Fjellvåg[b], Bjørn C. Hauback[a]

[(a)] Department for Neutron Materials Characterization, Institute for Energy Technology, P.O. Box 40, NO-2027 Kjeller, Norway
[(b)] Centre for Materials Science and Nanotechnology, University of Oslo, P.O. Box 1126, Blindern, NO-0318 Oslo, Norway
[(c)] Institute for Materials Research, Tohoku University, Sendai 980-8577, Japan
[(d)] WPI-Advanced Institute for Materials Research, Tohoku University, Sendai 980-8577, Japan

Abstract

Solid state electrolytic properties of mixtures of $Li(BH_4)_{0.75}I_{0.25}$ and amorphous $0.75Li_2S{\cdot}0.25P_2S_5$ are reported in this study. The enhanced Li-ion conductivities for the $Li(BH_4)_{0.75}I_{0.25}$ phase after addition of $0.75Li_2S{\cdot}0.25P_2S_5$ were found to be within the range for practical solid-state electrochemical storage near room temperature. The highest ionic conductivities are found for the borohydride/sulfide system at 1:2 weight ratio with ~10^{-3} S cm^{-1} at room temperature and an activation energy of 0.30(2) eV. Combined experimental analyses with powder X-ray diffraction and infrared/Raman spectroscopies suggest that the synthesized material still include both [PS_4^{3-}] and [BH_4^-] entities. Density functional theory (DFT) calculations provide more insights about the origin of the observed ionic behavior according to the induced structural modifications in the BH_4–BH_4 interactions. Finally, the electrolyte functionality and its compatibility toward an active material are successfully demonstrated by means of cyclic voltammetry (Au *vs.* Li^+/Li) in a large voltage window (up to 5 V) and battery cycling tests with TiS_2 electrode, respectively.

Keywords: solid-state electrolytes; borohydride-sulfide system; lithium batteries; ionic conductivity; DFT calculations

1. Introduction

The emerging applications for Li-ion batteries are very demanding regarding high energy density, reasonable lifespan, stability under extreme conditions such as wide temperature range, mechanical stress and fast solicitations for high power devices [1-4]. Solid electrolytes (SEs) can be beneficial in all these aspects compared to current liquid, gel or polymer-based electrolytes, for improved safety and performance of Li-ion batteries [5-9].

The glass system Li_2S-P_2S_5 has been extensively studied as electrolyte for application in all-solid-state Li-ion batteries [10-14]. However, these electrolytes have been reported to create unstable interface with Li [11,15]. The addition of lithium halides to Li_2S-P_2S_5 has been shown to increase the ionic conductivities and improve the contacts at the electrode/electrolyte interface [10,16]. Recently, the $LiBH_4$-Li_2S-P_2S_5 system has attracted attention owing to its adjustable ionic conductivity as function of composition for solid state battery electrolytes [17,18].

The crystal structure and ionic properties of $LiBH_4$ has been the subject of many reports [19-24]. It undergoes a first-order polymorphous transition around 113 °C, from orthorhombic (LT, *Pnma*, 10^{-8} S.cm^{-1} at 30 °C) to hexagonal (HT, *P6$_3$mc*, 10^{-3} S.cm^{-1} at 120 °C) involving a reorientation of the tetrahedral [BH_4^-] anions. High mobility of the complex anions [BH_4^-] in the HT-phase, along with short Li-Li distances in a compact structure with transport channels gave fast Li-ionic conduction [24-26]. Thus, $LiBH_4$ is a good Li-ion conductor between the phase transition temperature and the melting point at 280 °C, i.e. an operating domain less than ΔT=167 °C [22,27]. Below the transition temperature, the HT-phase reverts back to the poorly conducting LT-$LiBH_4$. However, the Li-ion conducting hexagonal phase can be stabilized by partly substituting [BH_4^-] with halides, e.g. $Li(BH_4)_{0.75}I_{0.25}$, thus suppressing the phase transition and preserving high ionic conductivity down to room temperature (*RT*), with a value close to 10^{-4} S cm^{-1} [28-31]. This phase has been reported to form a stable electrode/electrolyte interface in a lithium battery-cell [26,32].

The present work explores the effect of mixing crystalline hexagonal Li-ion conducting $Li(BH_4)_{0.75}I_{0.25}$ (LI) with amorphous $0.75Li_2S{\cdot}0.25P_2S_5$ (LPS) for solid-state electrolyte applications. The prepared electrolytes were investigated with respect to their structural and ionic properties and application for all-solid-state batteries. The experimental analytical investigations

are supported by DFT calculations to gain better understanding of the nature of the interaction between LI and LPS.

2. Experimental

2.1. Materials synthesis and characterization

$LiBH_4$ (95%), LiI (99.9%), Li_2S (99.98%) and P_2S_5 (99%) were purchased from Sigma-Aldrich and stored in an Ar-filled glove box (<1 ppm O_2, H_2O). The halide-stabilized hexagonal phase $Li(BH_4)_{0.75}I_{0.25}$ was synthesized according to the procedures described elsewhere [33]. The amorphous $0.75Li_2S{\cdot}0.25P_2S_5$ was prepared by ball-milling for 20 h using a Fritsch Pulverisette 6 (P6) planetary ball-mill with stainless steel vials and balls (ball-to-powder ratio 40:1, 300 or 370 rpm) [15,28,34]. The final electrolytes were obtained by mixing the two precursors LI/LPS at different wt. ratios using P6 planetary milling for 5 hours at 370 rpm.

Synchrotron radiation powder X-ray diffraction (SR-PXD) patterns were obtained at the Swiss-Norwegian Beamlines (SNBL, BM01), ESRF, Grenoble with a Pilatus2M 2-dimensional detector and a wavelength of 0.7454 Å. The samples were contained in 0.5 mm boronglass capillaries that were rotated 90 degrees during the 30 second exposure. The sample-detector distance was 345.97 mm. 1D data were obtained by integration of the 2D diffraction patterns with the program Bubble [35]. Lab-PXD data were obtained with a Bruker AXS D8 Advance diffractometer equipped with a Göbbel mirror and a LynxEye 1D strip detector. In this case, patterns were obtained in a Debye–Scherrer geometry using Cu Kα radiation (1.5418 Å) and rotating glass capillaries, filled and sealed under Ar atmosphere. The PXD data were analyzed using DIFFRAC.SUITE EVA software.

Attenuated total reflection Fourier transform infrared (ATR-FTIR) spectra were collected with a Bruker Alpha-Platinum spectrometer with a diamond crystal. The spectra were obtained in the range of 4000–400 cm^{-1} with a resolution of 2 cm^{-1}. The samples were measured without any dilution inside an Ar-filled glove box. IR spectra were ATR-corrected and normalized using the OPUS software. Further characterizations of the vibrational states were performed by Raman

spectroscopy (Nicolet Almega-HD, Thermo Scientific) using a dedicated cell without any air exposure.

2.2. Electrochemical analysis and battery tests

Ionic conductivities were determined by electrochemical impedance spectroscopy (EIS). The powder samples were pressed into 8 mm diameter pellet of < 2 mm thickness by a uniaxial press at around 240 MPa without sintering. The pellets were sandwiched by lithium foils as non-blocking electrodes and sealed in a homemade cell [36] for measurements outside the glovebox. The cells were placed in the heating jacket and the EIS were carried out over a frequency range from 1 MHz to 4 Hz using a HIOKI 3532-80 from *RT* to 150 °C in heating and cooling runs. Measured impedance spectra were analyzed by equivalent circuits using ZView2 software (Scribner Associates Inc.). Additional EIS measurements and cyclic voltammetry were performed using Bio-Logic® VSP multi-channel potentiostat, either in coin cells or a home-made cell described elsewhere [37].

For battery tests, TiS_2 (99.9%, Sigma-Aldrich) and Li foil were used as working and counter/reference electrode, respectively. The TiS_2 and the prepared SE powders in 2:3 mass ratio were hand mixed in an agate mortar. The obtained mixture was used as the electrode composite. Around 6 mg of this composite and 30 mg of the SE were introduced in a 10 mm die set and uniaxially pressed together at 240 MPa. A Li foil was placed on the opposite side of the electrode composite before the pellet was inserted in a coin cell. The assembled cells were moved out of glovebox and annealed at 60 °C for 5 h before testing at the cycling station (Bio-Logic instrument) in a temperature-controlled cabinet at 50 °C.

3. Computational details

Total energies were calculated by the projected-augmented plane-wave (PAW) implementation of the Vienna *ab initio* simulation package (VASP) [38,39]. These calculations were made with the Perdew, Burke, and Ernzerhof (PBE) exchange correlation functional [40]. Ground-state geometries were determined by minimizing stresses and Hellman-Feynman forces using the

conjugate-gradient algorithm with force convergence less than 10^{-3} eV $Å^{-1}$. Brillouin zone integration was performed with a Gaussian broadening of 0.1 eV during all relaxations. From various sets of calculations it was found that 512 **k** points in the whole Brillouin zone for the structure with a 600 eV plane-wave cut-off are sufficient to ensure optimum accuracy in the computed results. The **k**-points were generated using the Monkhorst-Pack method with a grid size of 8×8×8 for structural optimization. A similar density of **k**-points and energy cut-off were used to estimate total energy as a function of volume for all the structures considered in the present study. Iterative relaxation of atomic positions was stopped when the change in total energy between successive steps was less than 1 meV/cell. For the *ortho*-$LiBH_4$ (*Pnma*) and *hexa*-$LiBH_4$ (*P6$_3$mc*) phases the calculated lattice parameters (see SI. Table ST 1 and 2) are found to be in good agreement with experimental data. The lithium diffusion barrier height of the studied phase was investigated with the cNEB method using supercell approach [41,42]. Large supercells (2 X 2 X 1 for both *orthorhomic* and *hexagonal* phases) were used to ensure that the atoms were separated from their periodic image, providing a more accurate output values for the activation barrier in the diluted limit. To determine the minimum energy path (MEP) through the climbing Nudged Elastic Band (cNEB) method, six replicas of the system were created, in each the diffusing Li atom was moved by equidistant steps to positions between the initial and final states for the path obtained by linear interpolation.

4. Results and discussion

Fig. 1a presents lab-PXD patterns of $0.75Li_2S{\cdot}0.25P_2S_5$ samples before and after mechanical milling. The hand mixed sample shows Bragg peaks from Li_2S and P_2S_5 without any noticeable peaks from any reaction products. After ball-milling, an amorphous phase with no Bragg peaks is formed in agreement with previous studies [15]. Ionic conductivity measurements were performed on 2 different LPS batches prepared at different ball-milling conditions, i.e. rotation speed 300 and 370 rpm. The high energy (370 rpm) ball-milled LPS batch shows the highest conductivity and was retained for this study. We believe that the energy of ball-milling has a direct effect on the crystallite size and amorphization process, which may influence the resistance contributions of bulk and grain boundaries.

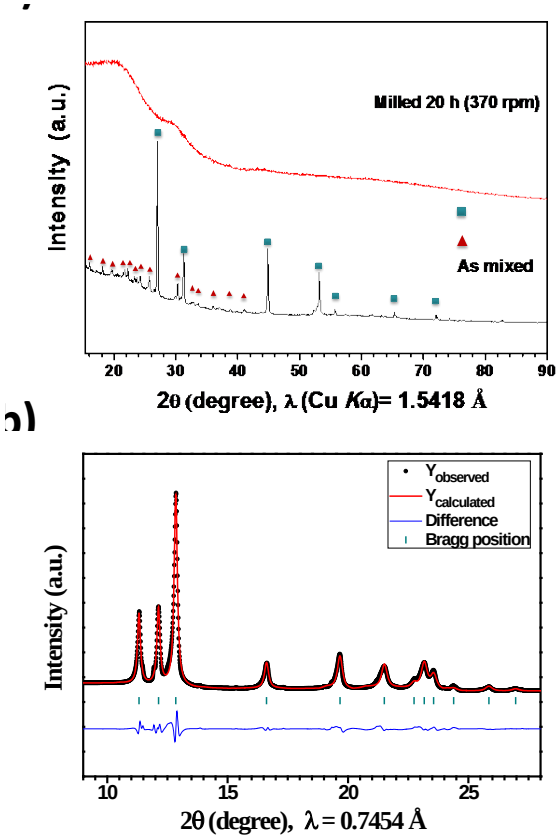

Fig. 1. PXD patterns of (a) $0.75Li_2S{\cdot}0.25P_2S_5$ as mixed (black) and after milling (red, shifted upwards for clarity) and (b) Rietveld fit to SR-PXD of the synthesized $Li(BH_4)_{0.75}I_{0.25}$.

The SR-PXD of the synthesized LI hexagonal phase (space group $P6_3mc$, refined lattice parameters a=4.3646(2) Å, c=7.0562(5) Å) is shown in Fig. 1b. The Rietveld refinement shows that LI is the only crystalline phase in the material. This LI phase was then added to the amorphous LPS at three weight fractions α = 0.67, 0.5 and 0.33 in αLI-(1-α)LPS. Fig. 2a shows the composition-dependent ionic conductivities at *RT*. The material with α = 0.33 (~mol. ratio 1:1) has a markedly higher conductivity than the others, and about one order of magnitude higher compared to LI or LPS alone. Similar tendency has been also reported when mixing two systems [15,43-45]. The overall ionic conductivity firstly increases with the addition of LI up to α = 0.33, and then decreases with the increased amount of LI. The corresponding EIS recorded for the different compositions are presented in Fig. 2b. The impedance spectra typically consist of an

intercept at high frequency with the ReZ axis, one depressed semicircle at medium frequency, and a low-frequency tail representing the electrode polarization due to the slow interfacial kinetics and non-ideal electrolyte/Li contacts. Insets show their corresponding equivalent circuits. An ohmic resistance (Rs-bulk) instead of parallel RC is used to represent the bulk of the electrolyte composite, which is similar to what was previously reported for several super ionic conductors [46-48]. While the compositions α = 0.33 and 0.5 show one slightly depressed semicircle attributed to grain boundary resistance (R_{gb}), an additional semicircle for α = 0.67 appears. Considering its characteristic frequency (330 Hz) and the corresponding effective capacitance (~ 30 μF obtained using $f_c = 1/2\pi RC$), we attribute this contribution to the interface resistance between the phases LI and LPS, probably due to their morphology difference and poor contacts in as-milled samples. Further study on the evolution of ionic conductivity and individual contribution as a function of temperature are needed to clarify the detailed mechanism.

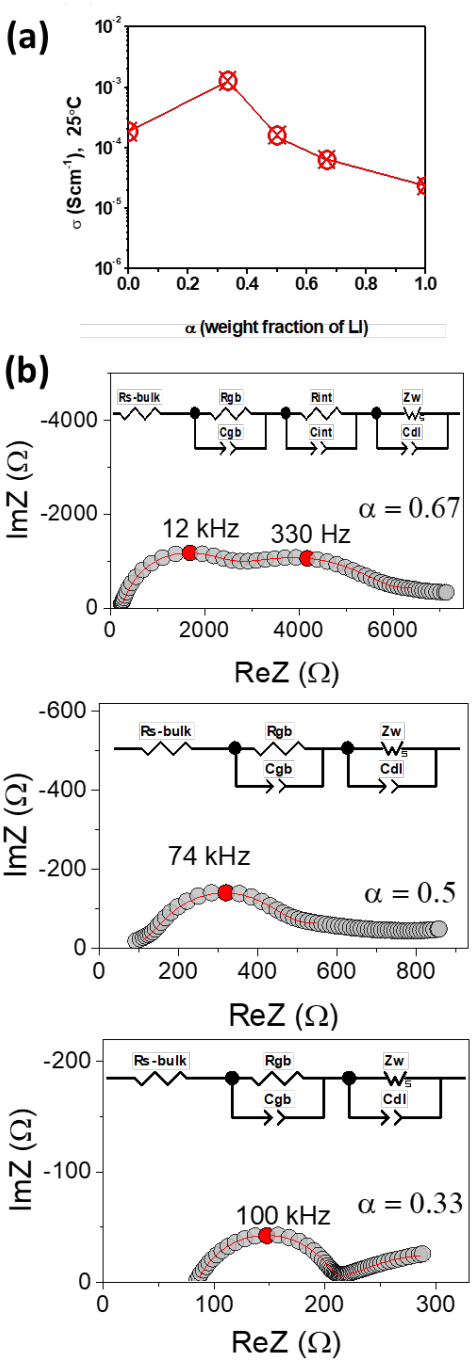

Fig. 2. Ionic conductivities (a) and Nyquist plots (b) of the LI/LPS system as function of composition at 25 °C. Insets are the corresponding equivalent circuits and red lines represent the fitting results.

Further characterization focuses on the composition α = 0.33 to get more details on the nature of the LI-LPS interaction. Fig. 3 presents the *in-situ* SR-PXD of this LI/LPS solid electrolyte as function of temperature upon heating with 10 °C min^{-1}. Before heating, the sample shows only Bragg peaks from LI at *RT* slightly shifted toward higher angles compared to the pure LI (Fig.1), as well as pronounced diffuse scattering from the amorphous component. A new phase is formed around 130 °C with peaks that cannot be assigned to any phase in the PDF-4 2016 database. Due to the limited number of peaks, indexing was not successful. Besides, the observed irreversibility of the process upon cooling down to *RT*, DSC/TGA analysis shows a small and wide endothermic event in the temperature range 50-150 °C without any significant gas release (Fig. S1 in Supplementary Information (SI) section).

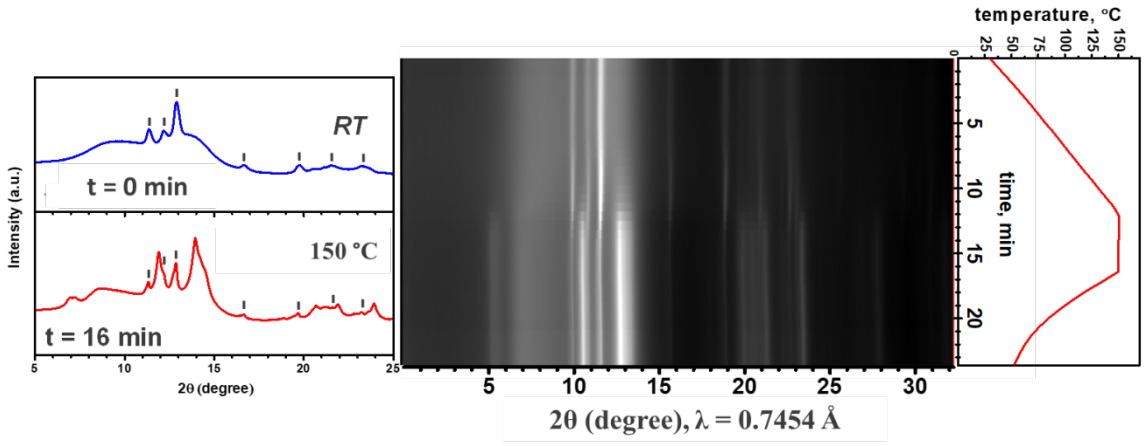

Fig. 3. *In-situ* SR-PXD of the LI/LPS (α = 0.33) as function of heating temperature from *RT* to 150 °C (10 °C min^{-1}). The patterns of the measurements at *RT* and 150 °C are given on the left side of the main figure. Peaks from hexanonal LI are indicated by vertical tick marks.

The temperature dependent ionic conductivities of LI/LPS (α = 0.33) were measured in the temperature range *RT*-150°C (Fig. 4). Remarkable ionic conductivity is obtained for this composition of about 10^{-3} S cm^{-1} near *RT*. The present result may have a direct implication on the development of solid-state batteries within a wide temperature range which cannot be

allowed via the commercial carbonate-based liquid electrolytes. The measurements showed some hysteresis in the first 2 heating/cooling cycles, but were stable with no hysteresis after the 3rd cycle (superimposed data points). Hence, only the conductivities inferred from AC impedance runs for the 3rd heating are shown in Fig. 4.

For the selected LPS system, the conductivities are slightly higher than the LI phase near *RT*, which converge to approximately the same conductivity levels beyond 120 °C. The measured values are in good agreement with the reported ones for LI and LPS single systems [15,17]. The recorded ionic conductivities for the *in-situ* heat-treated LI/LPS system (α = 0.33) increase gradually as expected as a function of temperature without any indication of phase transition. The obtained conductivities follow an Arrhenius trend according to the relation: $\sigma T = \sigma_0 \exp\left(-\frac{E_a}{kT}\right)$, where σ is the ionic conductivity and E_a the activation energy. The calculated E_a for α = 0.33 is 0.30 (2) eV.

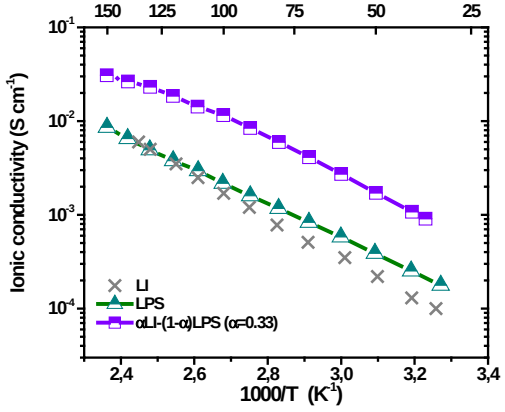

Fig. 4. Temperature dependence of the ionic conductivities for $0.75Li_2S$-$0.25P_2S_5$ before and after addition of $Li(BH_4)_{0.75}I_{0.25}$ (all data correspond to the 3rd heating ramps, which match well those obtained during cooling without any hysteresis).

Infrared spectroscopy has been carried out to shed light on the nature of the new chemical surroundings of BH_4 and possible interaction between the LI phase and the sulfur-based amorphous phase during mechanical milling and subsequent heat treatment. ATR-FTIR spectra for the three samples, 0.67, 0.5 and 0.33 wt. ratios as well as the single $LiBH_4$, LI and LPS systems are shown in Fig. 5a. The two characteristic bands (stretching and bending) of pure $LiBH_4$ can be seen in the 3000-400 cm^{-1} spectral region. The stretching band (1350-1000 cm^{-1}) is split in a wide region owing to the presence of an overtone ($3\nu_L$, 1231 cm^{-1}) assigned by Harvey and Mcquaker [49] to librational mode based on other alkali borohydrides. After halide incorporation, the intensity of the bands decreases and become less defined, as well as for the associated [BH_4^-] vibrational modes in accordance with previous works [29,50]. Progressively, the mixing with the LPS system at different proportions leads to weaker intensities and disappearance of some features of [BH_4^-] vibrational modes. However, the two main bands are still present and the lowered intensities may suggest a decrease of the symmetry and modified [BH_4^-] geometry. The presence of [PS_4^{3-}] entity is characterized by a wide peak at 542 cm^{-1} and is clearly observed in the spectrum of the pure amorphous LPS, likely due to the presence of the L_3PS_4 phase in the amorphous LPS [51]. The intensity of this vibrational structure decreases with increasing α in the mixed systems. This peak is slightly shifted toward higher wavenumbers for α = 0.33/0.5 (550 cm^{-1}) and α = 0.67 (558 cm^{-1}). Such feature can be attributed to the increase of the length of [PS_4^{3-}] chains as seen in similar amorphous mixtures [52]. Annealing the sample α = 0.33 for 24 h at 150 °C did not give any substantial changes in the FTIR spectra, except for the peak attributed to [PS_4^{3-}] group that becomes narrower and slightly more intense (not shown). This agrees with reduced configurational disorder after annealing. Fig. 5b shows Raman spectra of LPS and LI/LPS (α=0.33) before and after annealing. No additional information can be extracted for BH_4 groups for α=0.33. However, at low wavenumbers (inset Fig. 5b), Raman spectra confirm explicitly the presence of [PS_4^{3-}] moieties represented by the three peaks at 267, 422 and 564 cm^{-1} [17,47]. A shoulder can be seen at 385 cm^{-1} attributable to [$P_2S_6^{4-}$] ions [13], likely formed from a hypo-stoichiometric [PS_4^{3-}].

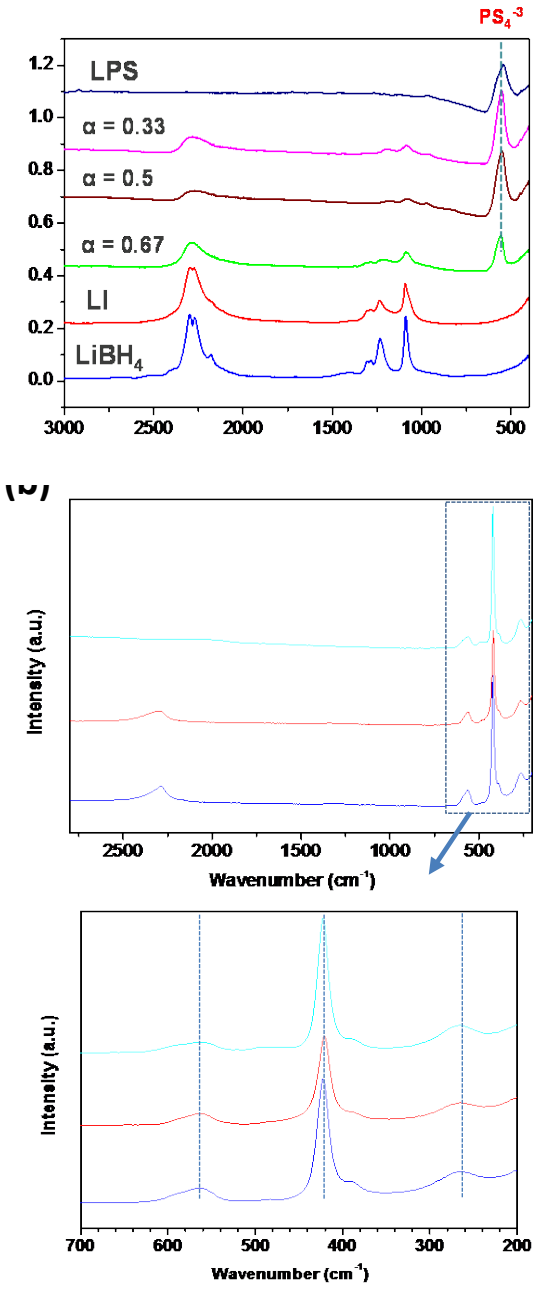

Fig. 5. (a) ATR-FTIR spectra of LI/LPS system at different ratios in the 3000-400 cm^{-1} region. (b) Raman spectra of LI/LPS (α = 0.33; as-milled and, further annealed) and LPS (α = 0). The spectral region 700-200 cm^{-1} is given as inset in the bottom of the figure for clarity.

Based on the observed DSC event described above in the *RT*-150 °C temperature range (Fig. S1), the observed irreversible transformation in the SR-PXD suggests a rearrangement of the BH_4 groups in the presence of $[PS_4^{3-}]$ and $[I^-]$ anions. This assumption is corroborated by the ATR-FTIR spectroscopic analysis where the BH_4 and PS_4 groups may co-exist in close environment. However, it is not possible from the present diffraction and IR data to establish if the different molecular entities are present in the crystalline and/or amorphous phases.

DFT calculations have been performed to better understand the nature of the structural influence which may exist between the Li dynamics and LPS addition. The aim of the calculations is to determine the energy barriers for Li ions jumping between different sites and how these barriers are influenced by incorporation of Li_2S and/or P_2S_5 molecular units and $[I^-]$ ions into the $LiBH_4$ structure. In this work, only the addition of the P_2S_5 phase to the LI system at low local concentration is considered, in order to have better view ability. The obtained results for the system *h*-$LiBH_4$+LiI+P_2S_5 are shown in Fig.6. After gradual structural modifications, meaning following the steps;

o-$LiBH_4$ → *h*-$LiBH_4$ → $Li(BH_4)_{0.75}I_{0.25}$ → $Li(BH_4)_{0.75}I_{0.25}{\cdot}P_2S_5$

the calculated activation barriers for the LT and HT phases of $LiBH_4$ are 0.69 eV and 0.53 eV respectively, in good agreement with previous theoretical works [22,24]. Upon introduction of LiI in the *h*-$LiBH_4$ matrix, these activation barriers are lower (0.42 eV to 0.54 eV) and the minimum values are found in proximity of the sites where BH_4^- is substituted by I^-. Similarly, upon introduction of P_2S_5 units in the *h*-$Li(BH_4)_{0.75}I_{0.25}$ matrix, the activation barriers are considerably lower, ranging from 0.19 eV to 0.63 eV. The lowest value is found in the proximity of the substituted P_2S_5 site, and the maximum one is observed at the second nearest BH_4 units from the P_2S_5 site. This finding clearly indicates that the Li mobility in $LiBH_4$ is mainly influenced by the interaction between the BH_4 - BH_4 molecular units. In both the HT and LT phase of $LIBH_4$ the interactions between the BH_4 - BH_4 molecular units are considerably larger, and they are hindering the transportation of lithium. In the case of HT polymorphs the Li are arranged in a layered structure, thus improving Li transportation. When $[I^-]$ or $[P_2S_5^{3-}]$ is substituted into the structure, the BH_4 - BH_4 interaction is reduced and more space is introduced, boosting the transportation of Li ions. This trend seems to be continued for increasing LPS ratio as shown in Fig. 2a. When the critical LPS ratio is reached, the opposite effect is observed, as the

BH_4 - BH_4 interaction is further reduced and interaction between P_2S_5 molecules arises, resulting in poorer Li transportation properties.

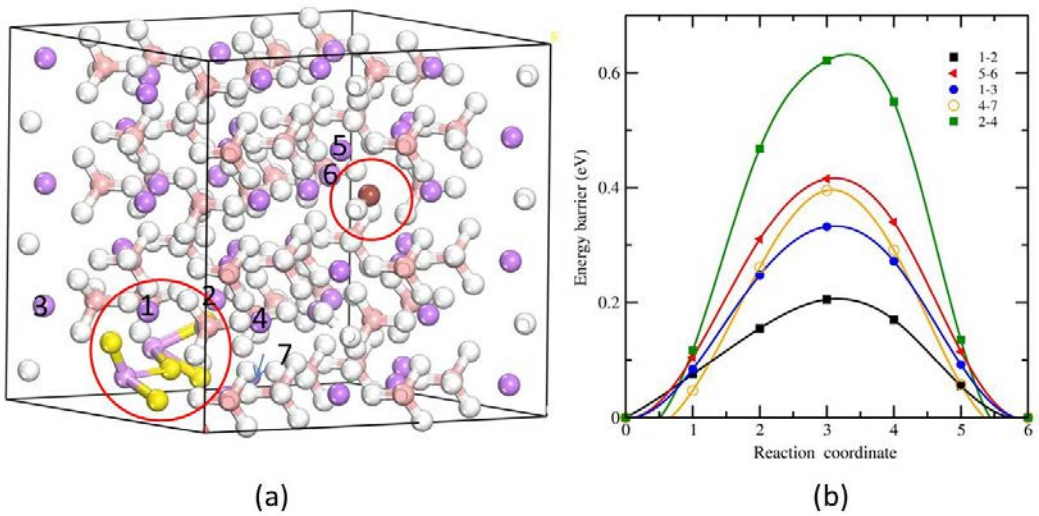

Fig. 6. Li ion migration in different possible path ways in (a) *h*-$LiBH_4$ doped with LiI and P_2S_5 as obtained from cNEB method and (b) energy barrier heights as function of the local concentration. The connected lines are given for visual help of the sequence of images. The symbols represent calculated data points.

The study is supplemented by transient electrochemical stability (*I-E*) measurements and battery tests at 50 °C for the best performing composition (α = 0.33). Prior to being used in a battery cell, the SE powders were homogenized by heat treatment at 150 °C for 24 h in reducing atm. (20 bar H_2) to avoid possible decomposition in these mixed systems. Cyclic voltammograms of the half-blocking cell Li │SE│Au (disc) are shown in Fig. 7a, in which the reversible stripping/platting of Li can be observed around 0 V with different scan rates. The composite electrolyte seems to show an electrochemical window up to 5 V. However, enlarged anodic part (inset) exhibits fluctuation of the CV curve mainly at slower scan rate with small anode peaks in the order of tens of nA per cm^2. This indicates possible existence of side reaction, for example oxidation reaction of residual polysulfide species, at the electrolyte/Li interface [53]. Nevertheless, these instabilities shown on the CV curve can be considered as minor processes since no significant reversible peak is observed [54]. Further CV characterization at lower scan rate using other

electrodes with better adhesion properties can help to distinguish the experimental noise and the stability level of this category of electrolytes.

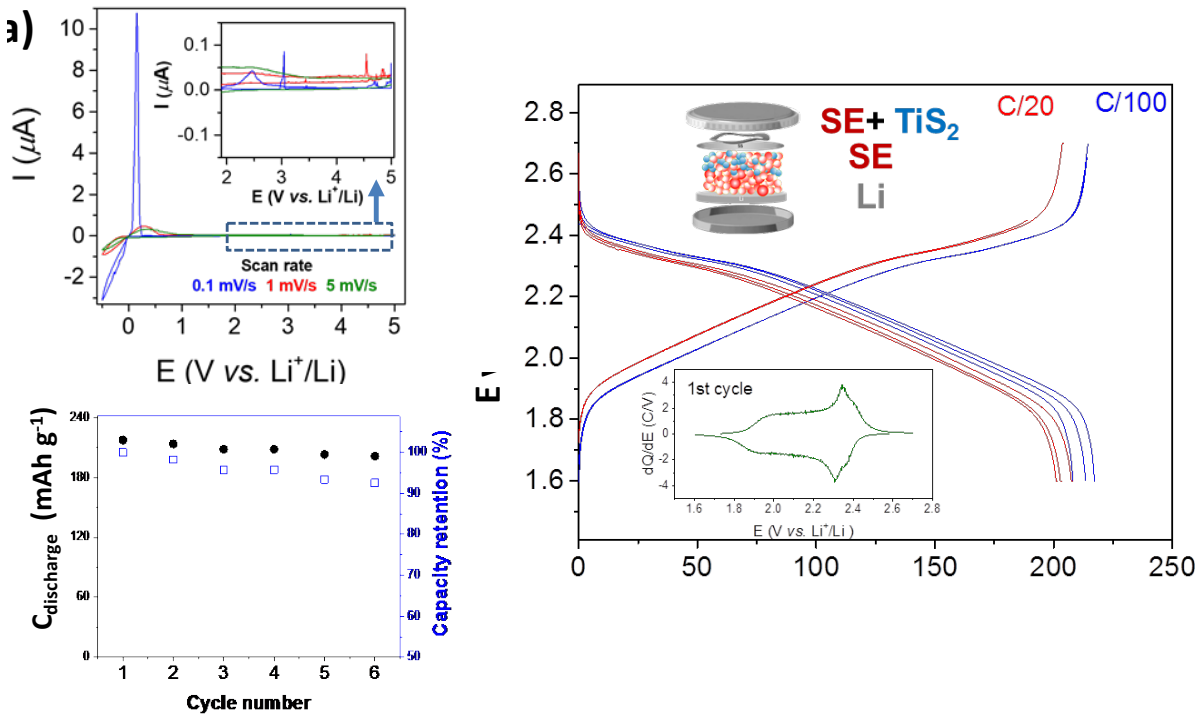

Fig. 7. Electrochemical characterization and performance of the selected solid electrolyte: (a) cyclic voltammetry at Au disc as working electrode *vs.* Li^+/Li (Inset: Y axis zoomed in to show the 2-5 V anodic region), (b) galvanostatic discharge/charge cycling with TiS_2 electrode at 50 °C (Inset: dQ/dE curve for the first cycle) and (c) discharge capacity (filled circles) and retention yield (open squares) as function of cycle number.

Using this optimized SE, battery tests were carried out with TiS_2 composite electrode in a Li-ion cell configuration. Fig. 7b shows the galvanostatic charge/discharge cycling, first at C/100 (3 cycles) and then followed by C/20 rates. The discharge capacity and capacity retention are presented in Fig. 7c as function of the cycle number, in which 91% of the theoretical capacity of TiS_2 (~239 mAh g^{-1}) is reached. It has been perceived that the cycling at low current during the first cycle helps to stabilize the electrode mechanical variations, as well as the electrode/electrolyte interface chemistry [55]. In fact, this activation process of the interfaces can avoid abrupt changes in the Ohmic drop owing to lack of contact and long Li diffusion pathways. Slight decrease of the capacity from C/100 to C/20 can be seen which is related to kinetic effect.

The following three discharge curves indicate a good cyclability and optimal coulombic efficiency. From one side, these tests are very promising as it shows repeatable cycling, mainly during the delithiation process for both experienced rates, meaning fast rechargeability can be expected. On the other hand, the lithiation emphasizes the good stability of the TiS_2 electrode toward the SE with no significant side reaction (differential curve, inset Fig. 7b) can be observed as far as the system remains almost fully reversible during cycling.

5. Conclusion

A novel strategy was followed to prepare a solid-sate electrolyte based on intimate mixing of crystalline $Li(BH_4)_{0.75}I_{0.25}$ (LI) with amorphous $0.75Li_2S{\cdot}0.25P_2S_5$ (LPS). The temperature dependence of the ionic conductivities were measured and optimized by varying the LI/LPS wt. ratio. The highest *RT* ionic conductivity ($\sim 10^{-3}$ S cm^{-1}) is found for the system with the approximate nominal composition $Li(BH_4)_{0.75}I_{0.25}{\cdot}(Li_2S)_{0.75}{\cdot}(P_2S_5)_{0.25}$. It has the lowest activation energy of the investigated LI/LPS systems in this study, 0.30(2) eV, in agreement with prediction of the DFT calculations. In this approach, it appears that mixing LI with LPS leads to high conduction resulting from structural modification of LI. Combined ATR-FTIR/Raman analyses and DFT calculations suggest that $[BH_4^-]$ groups are structurally influenced by the presence of $[PS_4^{3-}]$, likely as it does for the $[I^-]$ anions. This allows less hindered effect regarding Li mobility and consequently facilitating the Li ion conduction in the mixed system at lower temperature *RT* – 150 °C. In other words, when LPS is introduced the BH_4 - BH_4 interaction is reduced, and thus generating more freedom for Li mobility. However, after increasing the LPS ratio above a critical level, $[PS_4^{3-}]$ groups interact with each other, hindering Li transportation. During the preliminary electrochemical tests, this new SE is *a priori* stable in contact with Li metal and battery tests using TiS_2 electrodes show notable initial reversibility which is promising for further work on advanced battery tests including depth profile analysis of the electrode/electrolyte interface.

Acknowledgements

This work is financially supported by Research Council of Norway under the program EnergiX, Project no. 244054, LiMBAT - "Metal hydrides for Li-ion battery". PV acknowledges the Research Council of Norway for providing the computer time (under the project number NN2875k) at the Norwegian supercomputer. AE thanks Dr M. Heere for assistance with synchrotron data collection. We acknowledge the skillful assistance from the staff of SNBL at ESRF, Grenoble, France.

References

[1] M. Armand, J.M. Tarascon, Building better batteries, Nature 451 (2008) 652.
[2] J.B. Goodenough, Rechargeable batteries: challenges old and new, J. Solid State Electrochem. 16 (2012) 2019.
[3] E. Quartarone, P. Mustarelli, Electrolytes for solid-state lithium rechargeable batteries: recent advances and perspectives, Chem. Soc. Rev. 40 (2011) 2525.
[4] N. Legrand, B. Knosp, P. Desprez, F. Lapicque, S. Raël, Physical characterization of the charging process of a Li-ion battery and prediction of Li plating by electrochemical modelling, J. Power Sources 245 (2014) 208.
[5] C. Masquelier, Solid electrolytes: Lithium ions on the fast track, Nat. Mater. 10 (2011) 649.
[6] N. Kamaya, K. Homma, Y. Yamakawa, M. Hirayama, R. Kanno, M. Yonemura, T. Kamiyama, Y. Kato, S. Hama, K. Kawamoto, A. Mitsui, A lithium superionic conductor, Nat. Mater. 10 (2011) 682.
[7] M.H. Braga, N.S. Grundish, A.J. Murchison, J.B. Goodenough, Alternative strategy for a safe rechargeable battery, Energy Environ. Sci. 10 (2017) 331.
[8] A. Lecocq, G.G. Eshetu, S. Grugeon, N. Martin, S. Laruelle, G. Marlair, Scenario-based prediction of Li-ion batteries fire-induced toxicity, J. Power Sources 316 (2016) 197.
[9] Y. Wang, W.D. Richards, S.P. Ong, L.J. Miara, J.C. Kim, Y. Mo, G. Ceder, Design principles for solid-state lithium superionic conductors, Nat. Mater. 14 (2015) 1026.
[10] R. Mercier, J.-P. Malugani, B. Fahys, G. Robert, Superionic conduction in Li2S - P2S5 - LiI - glasses, Solid State Ionics 5 (1981) 663.
[11] M. Tatsumisago, S. Hama, A. Hayashi, H. Morimoto, T. Minami, New lithium ion conducting glass-ceramics prepared from mechanochemical Li2S–P2S5 glasses, Solid State Ionics 154–155 (2002) 635.
[12] F. Mizuno, A. Hayashi, K. Tadanaga, M. Tatsumisago, Design of composite positive electrode in all-solid-state secondary batteries with Li2S-P2S5 glass–ceramic electrolytes, J. Power Sources 146 (2005) 711.
[13] R.C. Xu, X.H. Xia, Z.J. Yao, X.L. Wang, C.D. Gu, J.P. Tu, Preparation of Li7P3S11 glass-ceramic electrolyte by dissolution-evaporation method for all-solid-state lithium ion batteries, Electrochim. Acta 219 (2016) 235.
[14] R. Garcia-Mendez, F. Mizuno, R. Zhang, T.S. Arthur, J. Sakamoto, Effect of Processing Conditions of 75Li2S-25P2S5 Solid Electrolyte on its DC Electrochemical Behavior, Electrochim. Acta 237 (2017) 144.
[15] A. Hayashi, S. Hama, H. Morimoto, M. Tatsumisago, T. Minami, Preparation of Li2S–P2S5 Amorphous Solid Electrolytes by Mechanical Milling, J. Am. Ceram. Soc. 84 (2001) 477.
[16] S. Ujiie, A. Hayashi, M. Tatsumisago, Structure, ionic conductivity and electrochemical stability of Li2S–P2S5–LiI glass and glass–ceramic electrolytes, Solid State Ionics 211 (2012) 42.
[17] A. Yamauchi, A. Sakuda, A. Hayashi, M. Tatsumisago, Preparation and ionic conductivities of $(100-x)(0.75Li_2S\cdot 0.25P_2S_5)\cdot xLiBH_4$ glass electrolytes, J. Power Sources 244 (2013) 707.
[18] A. Unemoto, H. Wu, T.J. Udovic, M. Matsuo, T. Ikeshoji, S.-i. Orimo, Fast lithium-ionic conduction in a new complex hydride-sulphide crystalline phase, Chem. Commun. 52 (2016) 564.
[19] J.P. Soulié, G. Renaudin, R. Cerný, K. Yvon, Lithium boro-hydride LiBH4: I. Crystal structure, J. Alloys Compd. 346 (2002) 200.
[20] Y. Filinchuk, D. Chernyshov, R. Cerny, Lightest Borohydride Probed by Synchrotron X-ray Diffraction: Experiment Calls for a New Theoretical Revision, J. Phys. Chem. C 112 (2008) 10579.
[21] P. Vajeeston, P. Ravindran, A. Kjekshus, H. Fjellvåg, Structural stability of alkali boron tetrahydrides ABH4 (A = Li, Na, K, Rb, Cs) from first principle calculation, J. Alloys. Compd. 387 (2005) 97.
[22] M. Matsuo, Y. Nakamori, S.-i. Orimo, H. Maekawa, H. Takamura, Lithium superionic conduction in lithium borohydride accompanied by structural transition, Appl. Phys. Lett. 91 (2007) 224103.
[23] T. Ikeshoji, E. Tsuchida, K. Ikeda, M. Matsuo, H.-W. Li, Y. Kawazoe, S.-i. Orimo, Diffuse and doubly split atom occupation in hexagonal LiBH4, Appl. Phys. Lett. 95 (2009) 221901.

[24] T. Ikeshoji, E. Tsuchida, T. Morishita, K. Ikeda, M. Matsuo, Y. Kawazoe, S.-i. Orimo, Fast-ionic conductivity of Li in LiBH4, Phys. Rev. B 83 (2011) 144301.
[25] V. Epp, M. Wilkening, Fast Li diffusion in crystalline LiBH4 due to reduced dimensionality: Frequency-dependent NMR spectroscopy, Phys. Rev. B 82 (2010) 020301.
[26] M. Matsuo, S.-i. Orimo, Lithium Fast-Ionic Conduction in Complex Hydrides: Review and Prospects, Adv. Energy Mater. 1 (2011) 161.
[27] A. El kharbachi, I. Nuta, F. Hodaj, M. Baricco, Above room temperature heat capacity and phase transition of lithium tetrahydroborate, Thermochim. Acta 520 (2011) 75.
[28] R. Miyazaki, T. Karahashi, N. Kumatani, Y. Noda, M. Ando, H. Takamura, M. Matsuo, S. Orimo, H. Maekawa, Room temperature lithium fast-ion conduction and phase relationship of LiI stabilized LiBH4, Solid State Ionics 192 (2011) 143.
[29] L.H. Rude, E. Groppo, L.M. Arnbjerg, D.B. Ravnsbæk, R.A. Malmkjær, Y. Filinchuk, M. Baricco, F. Besenbacher, T.R. Jensen, Iodide substitution in lithium borohydride, LiBH4–LiI, J. Alloys Compd. 509 (2011) 8299.
[30] D. Sveinbjörnsson, J.S.G. Myrdal, D. Blanchard, J.J. Bentzen, T. Hirata, M.B. Mogensen, P. Norby, S.-I. Orimo, T. Vegge, Effect of Heat Treatment on the Lithium Ion Conduction of the LiBH4–LiI Solid Solution, J. Phys. Chem. C 117 (2013) 3249.
[31] H. Maekawa, M. Matsuo, H. Takamura, M. Ando, Y. Noda, T. Karahashi, S.-i. Orimo, Halide-Stabilized LiBH4, a Room-Temperature Lithium Fast-Ion Conductor, J. Am. Chem. Soc. 131 (2009) 894.
[32] A. Unemoto, M. Matsuo, S.-i. Orimo, Complex Hydrides for Electrochemical Energy Storage, Adv. Funct. Mater. 24 (2014) 2267.
[33] K. Yoshida, S. Suzuki, J. Kawaji, A. Unemoto, S. Orimo, Complex hydride for composite negative electrode—applicable to bulk-type all-solid-state Li-ion battery with wide temperature operation, Solid State Ionics 285 (2016) 96.
[34] A. Unemoto, K. Yoshida, T. Ikeshoji, S.-i. Orimo, Bulk-Type All-Solid-State Lithium Batteries Using Complex Hydrides Containing Cluster-Anions, Mater. Trans. 57 (2016) 1639.
[35] V. Dyadkin, P. Pattison, V. Dmitriev, D. Chernyshov, A new multipurpose diffractometer PILATUS@SNBL, J. Synchrotron Rad. 23 (2016) 825.
[36] U. Atsushi, C. ChunLin, W. Zhongchang, M. Motoaki, I. Tamio, O. Shin-ichi, Pseudo-binary electrolyte, LiBH 4 –LiCl, for bulk-type all-solid-state lithium-sulfur battery, Nanotechnology 26 (2015) 254001.
[37] A. El kharbachi, Y. Hu, M.H. Sørby, P.E. Vullum, J.P. Mæhlen, H. Fjellvåg, B.C. Hauback, Understanding Capacity Fading of MgH2 Conversion-Type Anode via Structural Morphology Changes and Electrochemical Impedance, J. Phys. Chem. C (2018) https://doi.org/10.1021/acs.jpcc.7b12656.
[38] G. Kresse, J. Furthmüller, Efficient iterative schemes for *ab initio* total-energy calculations using a plane-wave basis set, Phys. Rev. B 54 (1996) 11169.
[39] G. Kresse, J. Furthmüller, Efficiency of ab-initio total energy calculations for metals and semiconductors using a plane-wave basis set, Comput. Mater. Sci. 6 (1996) 15.
[40] J.P. Perdew, K. Burke, M. Ernzerhof, Generalized Gradient Approximation Made Simple, Phys. Rev. Lett. 77 (1996) 3865.
[41] G. Henkelman, H. Jónsson, Improved tangent estimate in the nudged elastic band method for finding minimum energy paths and saddle points, J. Chem. Phys. 113 (2000) 9978.
[42] H. Jónsson, G. Mills, K.W. Jacobsen, Proc. Classical and Quantum Dynamics in Condensed Phase Simulations, 2011.
[43] M. Tachez, J.-P. Malugani, R. Mercier, G. Robert, Ionic conductivity of and phase transition in lithium thiophosphate Li3PS4, Solid State Ionics 14 (1984) 181.
[44] M. Tatsumisago, A. Hayashi, Superionic glasses and glass–ceramics in the Li2S–P2S5 system for all-solid-state lithium secondary batteries, Solid State Ionics 225 (2012) 342.
[45] J.H. Kennedy, Y. Yang, A Highly Conductive Li+ Glass System: (1−x) (0.4SiS2 ‐ 0.6Li2S) ‐ xLil, J. Electrochem. Soc. 133 (1986) 2437.

[46] N. Kamaya, K. Homma, Y. Yamakawa, M. Hirayama, R. Kanno, M. Yonemura, T. Kamiyama, Y. Kato, S. Hama, K. Kawamoto, A. Mitsui, A lithium superionic conductor, Nature Mater. 10 (2011) 682.
[47] A. Kuhn, O. Gerbig, C. Zhu, F. Falkenberg, J. Maier, B.V. Lotsch, A new ultrafast superionic Li-conductor: ion dynamics in Li11Si2PS12 and comparison with other tetragonal LGPS-type electrolytes, Phys. Chem. Chem. Phys. 16 (2014) 14669.
[48] O. Kwon, M. Hirayama, K. Suzuki, Y. Kato, T. Saito, M. Yonemura, T. Kamiyama, R. Kanno, Synthesis, structure, and conduction mechanism of the lithium superionic conductor Li10+[small delta]Ge1+[small delta]P2-[small delta]S12, J. Mater. Chem. A 3 (2015) 438.
[49] K.B. Harvey, N.R. McQuaker, Low Temperature Infrared and Raman Spectra of Lithium Borohydride, Can. J. Chem. 49 (1971) 3282.
[50] L.H. Rude, O. Zavorotynska, L.M. Arnbjerg, D.B. Ravnsbæk, R.A. Malmkjær, H. Grove, B.C. Hauback, M. Baricco, Y. Filinchuk, F. Besenbacher, T.R. Jensen, Bromide substitution in lithium borohydride, LiBH4–LiBr, Int. J. Hydrogen Energy 36 (2011) 15664.
[51] H. Muramatsu, A. Hayashi, T. Ohtomo, S. Hama, M. Tatsumisago, Structural change of Li2S–P2S5 sulfide solid electrolytes in the atmosphere, Solid State Ionics 182 (2011) 116.
[52] P. Berthet, E. Bretey, J. Berthon, F. d'Yvoire, A. Belkebir, A. Rulmont, B. Gilbert, Structure and ion transport properties of Na2O-Ga2O3-P2O5 glasses, Solid State Ionics 70-71 (1994) 476.
[53] K. Minami, A. Hayashi, S. Ujiie, M. Tatsumisago, Electrical and electrochemical properties of glass–ceramic electrolytes in the systems Li2S–P2S5–P2S3 and Li2S–P2S5–P2O5, Solid State Ionics 192 (2011) 122.
[54] R.-c. Xu, X.-h. Xia, X.-l. Wang, Y. Xia, J.-p. Tu, Tailored Li2S-P2S5 glass-ceramic electrolyte by MoS2 doping, possessing high ionic conductivity for all-solid-state lithium-sulfur batteries, J. Mater. Chem. A 5 (2017) 2829.
[55] A. Unemoto, T. Ikeshoji, S. Yasaku, M. Matsuo, V. Stavila, T.J. Udovic, S.-i. Orimo, Stable Interface Formation between TiS2 and LiBH4 in Bulk-Type All-Solid-State Lithium Batteries, Chem. Mater. 27 (2015) 5407.